

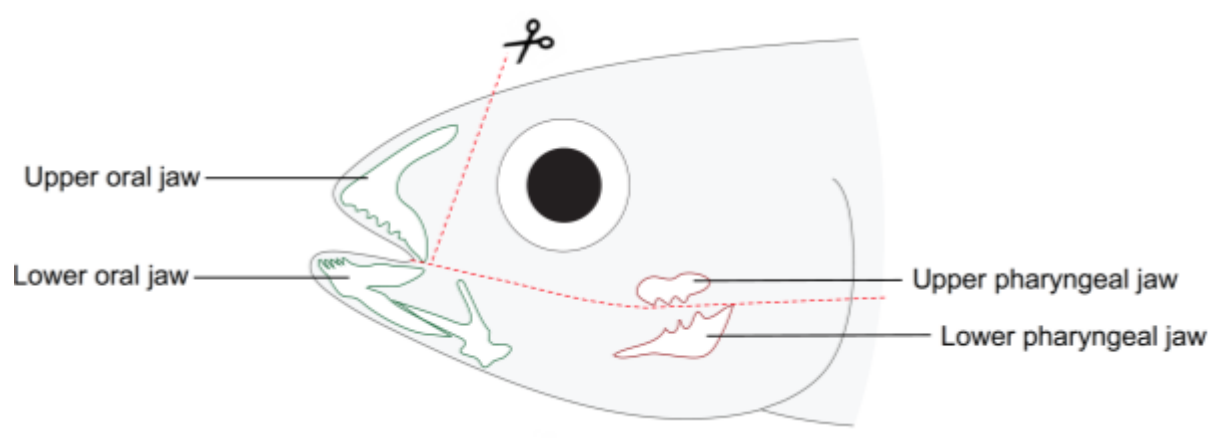
Supplementary information,

Singh *et al.*

Table of Contents

Supplementary information,	1
1. Dissection strategy	2
Supplementary Figure 1	2
2. 2D geometric morphometric analysis	2
Method.....	2
Supplementary Table 1	3
Supplementary Figure 2	4
Results	4
Supplementary Figure 3	6
Discussion	7
3. Gene Ontology analysis	7
Supplementary Table 2.....	7
4. RNA-seq analysis	8
Supplementary Figure 4	8
References	8

1. Dissection strategy



Supplementary Figure 1

Schematic depiction of the dissection strategy utilised in this study. Red dotted lines mark the cuts made. The upper and lower oral jaws and the lower pharyngeal jaw constituted the ‘lower suspensorium’ that was used for RNA-extraction. The dissection included the following tissues: bone, cartilage, teeth, muscle, tendons, fat, and blood vessels.

2. 2D geometric morphometric analysis

Method

A Scanco μ CT 40 (SCANCO Medical AG, Brüttisellen, Switzerland) collected a series of two-dimensional micro-computed tomography (micro-CT) images of the head of each fish with a resolution of either 2 or 10 $\mu\text{m}/\text{pixel}$. We isolated regions of the resulting .tiff images showing the head of the fish, and simultaneously converted them to DICOM images, using custom-written software (Matlab R2011b, The MathWorks, Inc., Natick, MA, USA). From these, the TINA Geometric Morphometrics Toolkit generated three-dimensional reconstructions of the bones in each fish’s head (Schunke *et al.* 2012); we down-sampled the 2 $\mu\text{m}/\text{pixel}$ scans fivefold, so that all reconstructions had a voxel size of 10 μm . Reconstructions were rendered using the surface rendering style shipped with TINA (tmlt_surface_style.txt), with thresholds adjusted as needed to show all jaw bone features. We rotated each reconstruction to show a lateral view of the head, superimposing the left and right otoliths and jaw bones. The dump function of TINA exported a two-dimensional screenshot of the three-dimensional reconstruction as a tiff image, which we converted to bitmap.

TpsUtil (ver. 1.64; Rohlf 2015) built a randomized tps file from the bitmap images. We used tpsDig2 (ver. 2.30; Rohlf 2017) to set the scale of each image using the length of the TINA crosshairs as a standardized number of voxels. We placed a set of functionally-relevant landmarks and semi-landmarks on bones of the oral jaws (premaxilla, dentary, and articular) and the lower pharyngeal jaw using tpsDig2 (Suppl. Table 1, Suppl. Figure 2), referring to the corresponding three-dimensional reconstruction in TINA as a guide to accurately place each landmark. Next, we used tpsUtil to restore the original order of the specimens and to designate semi-landmarks by creating a sliders file. From the tps file and sliders file, tpsrelw32 (ver 1.60; Rohlf 2017b) performed a semi-landmark superimposition. We imported the aligned landmark set into MorphoJ (ver. 1.06d; Klingenberg 2011) with the centroid sizes as covariates, performed a Procrustes superimposition, then adjusted for allometry using a pooled within-species regression of Procrustes coordinates on centroid size (Klingenberg 2016). A permutation test using 10,000 permutations indicated a significant effect of specimen size on shape ($p=0.0007$), so we performed our final principle component analysis on the regression residuals to determine the shape changes responsible for variability in our specimens.

Supplementary Table 1

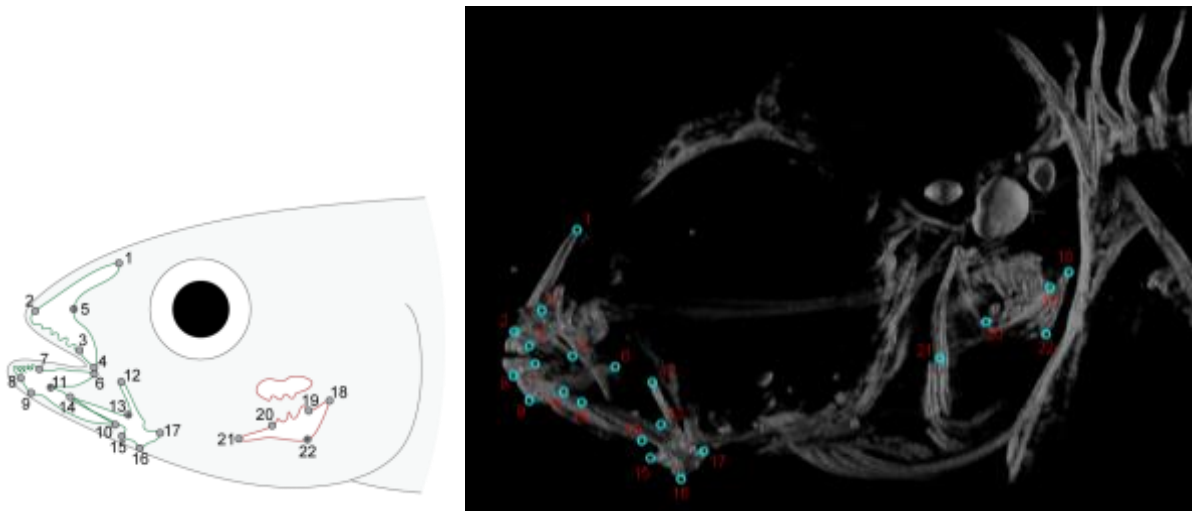
Landmarks and semi-landmarks used for geometric morphometrics of oral and pharyngeal jaw bones. Semi-landmarks are indicated with a superscript *. Terminology as in (Barel & van Oijen 1976). Landmarks are based on those in (Fujimura & Okada 2008; Kalt 2017; Powder *et al.* 2015).

Premaxilla	
1	Dorsal tip of ascending arm
2	Anterior tip (base of tooth)
3	Posterior end of dentiginous area (base of tooth)
4	Posterior tip of dentiginous arm
*5	Curve between dentiginous arm and ascending arm
Dentary	
6	Posterior tip of coronoid (dentary) process
7	Posterior end of dentiginous area (base of tooth)
8	Anterior tip (base of tooth)
9	Anterior ventral corner of chin
10	Posterior ventral tip
*11	Reentrant angle
Articular	
12	Dorsal tip of primordial (articular) process
*13	Posterior ventral border of dorsal obturated foramen

-
- 14 Anterior tip of articular excurvation
 - 15 Anterior process of coulter area
 - 16 Ventral tip of retroarticular process
 - 17 Postarticulation process of coulter area
-

Lower pharyngeal

- 18 Posterior end of horn
 - 19 Posterior end of dentiginous area (base of tooth)
 - 20 Anterior end of dentiginous area (base of tooth)
 - 21 Anterior tip of keel
 - *22 Center of ventral-most point
-



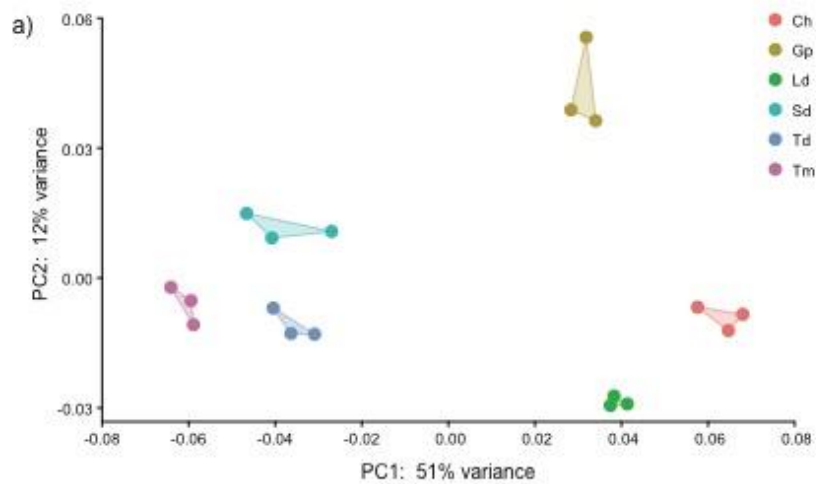
Supplementary Figure 2

Landmarks and semilandmarks for geometric morphometrics, shown schematically (left) and on a two-dimensional image of a three-dimensional reconstruction (right). Semilandmarks are denoted with crosshairs in the schematic image (left). See Supplementary Table 2 for landmark locations.

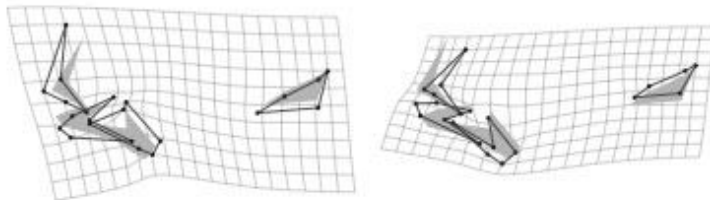
Results

Increasing PC1 loading was associated with the oral jaws closing and the mouth becoming more superior and upward-pointing; the premaxilla having a decreased angle between its ascending and dentiginous arms, and a shorter dentiginous area; the dorsal obturated foramen having a more acute angle at its posteroventral border (between the primordial process and articular excurvation); and the lower pharyngeal jaw having a shorter keel (Suppl. Figure 3b). Increasing PC2 loading was

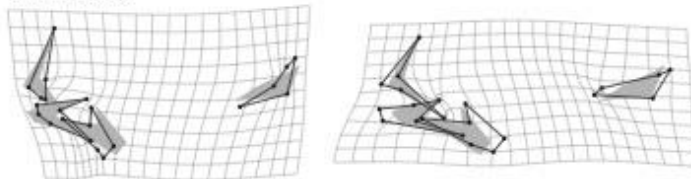
associated with the premaxilla having a longer dentiginous arm; the dentary having a longer dentiginous area; the articular having a longer anteroventral portion and anterior-posteriorly wider coulter area; and the lower pharyngeal jaw having a longer dentiginous area, shorter keel, and more horizontal orientation (Suppl. Figure 3c). Increasing PC3 loading was associated with the premaxilla having a longer dentiginous arm; the dentary having a longer dentiginous area and longer coronoid process; the dorsal obturated foramen having a more obtuse angle at its posteroventral border; the articular having a anterior-posteriorly narrower coulter area and more vertical alignment; and the lower pharyngeal jaw having longer, more dorsally-pointing, horns and more horizontal orientation (Suppl. Figure 3d).



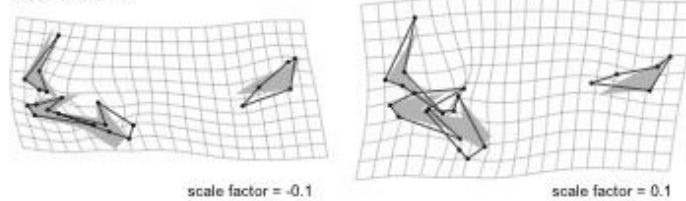
b) PC1: 51% variance



c) PC2: 12% variance



d) PC3: 10% variance



Supplementary Figure 3

Results of the principle component analysis on the landmarks of oral and pharyngeal jaw bones. (a) Plotting the first and second principle components (PC1 and PC2) shows individuals of the same species grouped together, with the two species that are algae browsing herbivores and one omnivorous species having negative PC1 loadings while the other omnivore and the two carnivorous species have positive PC2 loadings. (b)—(d) Deformation grids and wireframes for PC1—PC3, respectively, with the left column of plots having a scale factor of -0.1 and the right column having a scale factor of 0.1. Solid grey areas indicate the average (consensus) landmark configuration, while black lines indicate the deformed configuration and black filled circles indicate landmarks.

Discussion

Our morphometric analysis proved the morphological features of juvenile cichlids are similar to those previously described in adults – for example, the mouths of the carnivorous juveniles were less blunt and angled more superiorly compared to herbivores, as is seen in the external morphology of adults of the same species and other Great Lake cichlids (Cooper *et al.* 2010; Wanek & Sturmbauer 2015). This suggests that individuals have already acquired their species-specific adaptive features upon completion of larval development (stage 26). The oral jaw bones show pronounced differences between species, reflecting the diversity of methods employed to acquire food – species that bite off algae have shorter, more robust oral jaws to produce higher scraping forces than species that use suction to capture their prey (Albertson & Kocher 2001). The lower pharyngeal jaw showed the most noticeable differences between carnivorous species, likely reflecting the different hardnesses of their prey (Hulseley *et al.* 2006; Muschick *et al.* 2012). Our observed separation of species according to differences in prey capture and prey processing supports the idea that the oral and pharyngeal jaws specialise for different tasks (Liem 1973).

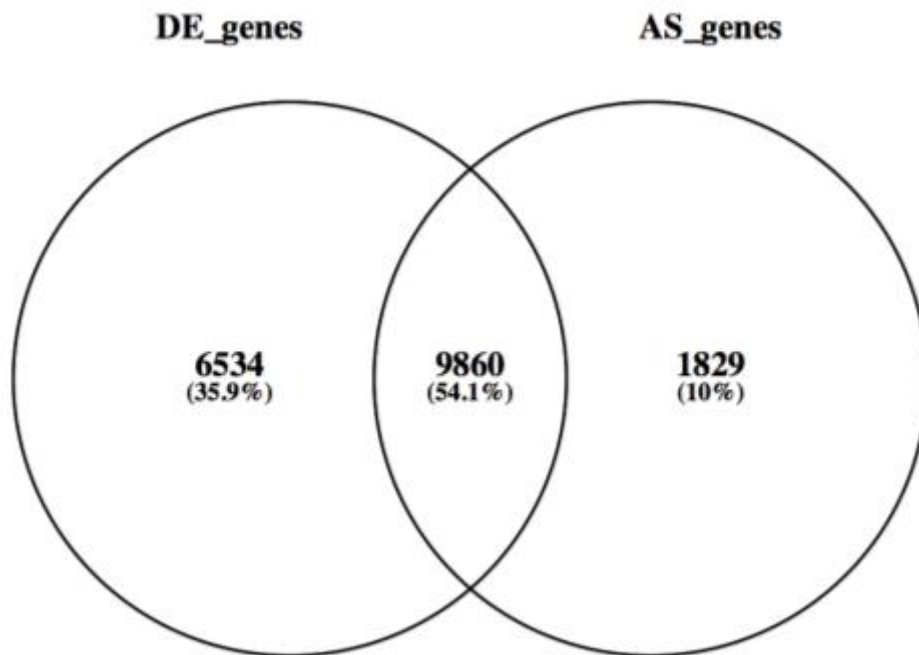
3. Gene Ontology analysis

Supplementary Table 2

Candidate genes that are alternatively spliced with “pharyngeal jaw system” GO term annotation.

<i>O. niloticus</i> gene ID	Ensemble ID	Gene name	Gene description
on.gene.LG11.793	ENSTNIG00000003926	PRDM1	PR domain containing 1, with ZNF domain
on.gene.LG12.131	ENSGACG00000013057	TBX1	T-box 1
on.gene.LG16-21.21	ENSGACG00000001456	PKNOX1	PBX/knotted 1 homeobox 1
on.gene.LG16-21.422	ENSORLG00000017372	dlx2a	dlx2a protein
on.gene.LG18.504	ENSTNIG00000008486	WNT9A	wingless-type MMTV integration site family, member 9A
on.gene.LG2.11	ENSGACG00000016847	SPARC	secreted protein, acidic, cysteine-rich (osteonectin)
on.gene.LG20.704	ENSORLG00000007861	A5JL88_ORYLA	Retinoic acid receptor gamma 1
on.gene.LG23.458	ENSORLG00000017140	FAF1	Fas (TNFRSF6) associated factor 1
on.gene.LG5.47	ENSGACG00000011231	BARX1	BARX homeobox 1
on.gene.UNK45.28	ENSTNIG00000006362	FGF8 (1 of 2)	fibroblast growth factor 8 (androgen-induced)

4. RNA-seq analysis



Supplementary Figure 4

Venn diagram of overlap between differentially expressed (DE) genes and alternatively spliced (AS) genes.

References

- Albertson CR, Kocher TD. 2001. Assessing morphological differences in an adaptive trait: a landmark-based morphometric approach. *J. Exp. Zool.* 289:385–403.
- Barel C, van Oijen M. 1976. The shape of the skeletal elements in the head of a generalized *Haplochromis* species: *H. Elegans* Trewavas 1933 (Pisces, Cichlidae). *Netherlands J. Zool.* 26:163–265.
- Cooper WJ *et al.* 2010. Benthic-pelagic divergence of cichlid feeding architecture was prodigious and consistent during multiple adaptive radiations within African rift-lakes. *PLoS One.* 5:e9551. doi: 10.1371/journal.pone.0009551.
- Fujimura K, Okada N. 2008. Shaping of the lower jaw bone during growth of Nile tilapia *Oreochromis niloticus* and a Lake Victoria cichlid *Haplochromis chilotes*: A geometric morphometric approach. *Dev. Growth Differ.* 50:653–663. doi: 10.1111/j.1440-169X.2008.01063.x.
- Hulsey CD, García de León FJ, Rodiles-Hernández R. 2006. Micro- and macroevolutionary decoupling of cichlid jaws: a test of Liem's key innovation hypothesis. *Evolution.* 60:2096–2109.
- Kalt JM. 2017. Geometric morphometric analysis from three-dimensional computer tomograms of

cichlid skulls. University of Graz.

Klingenberg CP. 2011. MORPHO J: an integrated software package for geometric morphometrics. *Mol. Ecol. Resour.* 11:353–357. doi: 10.1111/j.1755-0998.2010.02924.x.

Klingenberg CP. 2016. Size, shape, and form: concepts of allometry in geometric morphometrics. *Dev. Genes Evol.* 226:113–137. doi: 10.1007/s00427-016-0539-2.

Liem KF. 1973. Evolutionary strategies and morphological innovations: cichlid pharyngeal jaws. *Syst. Zool.* 22:425–441. doi: 10.2307/2412950.

Muschick M, Indermaur A, Salzburger W. 2012. Convergent evolution within an adaptive radiation of cichlid fishes. *Curr. Biol.* 22:2362–2368. doi: 10.1016/j.cub.2012.10.048.

Powder KE, Milch K, Asselin G, Albertson RC. 2015. Constraint and diversification of developmental trajectories in cichlid facial morphologies. *Evodevo.* 6:25. doi: 10.1186/s13227-015-0020-8.

Rohlf FJ. 2017a. tpsDig, digitize landmarks and outlines. 2.3 edition.

Rohlf FJ. 2017b. tpsRelw, relative warps analysis. 1.67 edition.

Rohlf FJ. 2015. tpsUtil, file utility program 1.64 edition.

Schunke AC, Bromiley PA, Tautz D, Thacker NA. 2012. TINA manual landmarking tool: software for the precise digitization of 3D landmarks. *Front. Zool.* 9:1–6. doi: 10.1186/1742-9994-9-6.

Wanek AK, Sturmbauer C. 2015. Form, function and phylogeny: comparative morphometrics of Lake Tanganyika's cichlid tribe Tropheini. *Zool. Scr.* 44:362–373. doi: 10.1111/zsc.12110.